Int. J. Heat Mass Transfer. Vol. 28, No. 7, 1327–1336, 1985
Printed in Great Britain

0017–9310/85 $3.00 + 0.00

Plasma–particle interaction effects in induction plasma modeling under dense loading conditions

PIERRE PROULX, JAVAD MOSTAGHIMI and MAHER I. BOULOS
Department of Chemical Engineering, University of Sherbrooke, Québec, Canada J1K 2R1

(*Received* 26 *June* 1984 *and in final form* 2 *January* 1985)

Abstract—The injection of powders into an inductively coupled plasma is modeled. Attention is given to the plasma–particle interaction and its effect on plasma fields. It is demonstrated that for most applications, such interactions must be considered in any model. For the calculations, copper and alumina powders are used. The plasma gas is argon at atmospheric pressure.

1. INTRODUCTION

THE STUDY of heat transfer to particles injected into thermal plasmas have been of considerable interest for some time. This interest stems from a variety of industrial applications, e.g. plasma spray coating, that makes the understanding of the basic processes involved in thermal treatment of powders in a plasma a necessity.

A complete mathematical modeling of the problem involves the prediction of the flow field and the temperature field in the plasma as well as the prediction of the particle trajectory and its temperature history. Generally the introduction of powders into a plasma will affect the flow and the temperature fields and therefore a rigorous treatment of this problem should in fact consider the coupling between the particle heating and the plasma fields.

Studies of heating powders in a DC plasma jet [1–3] and in inductively coupled plasmas [4–6] have neglected the plasma–particle interaction. While this is a reasonable assumption under low powder injection rate conditions, it is unlikely to be the case in most applications. For high powder injection rates, the presence of the powder will have two effects. First the heat extracted by the powder from the plasma could cause substantial local cooling of the gas. Secondly, depending on the type of powder, the evaporated fraction of the particles diffuses in the plasma gas, and can drastically change its thermodynamic and transport properties, e.g. electrical conductivity, of the plasma gas [7].

The objective of the present paper is to investigate these two aspects of the particle heating in an inductively coupled plasma torch. Copper and alumina particles are considered to be injected in an argon inductive coupled plasma under atmospheric pressure. For consideration of the plasma–particle interaction the so-called Particle-Source-In-Cell (PSI-Cell) method [8] is used.

2. THE MODEL

The proposed model is an extension of the work by Boulos [4] and of the procedure described by Mostaghimi *et al.* [9]. The plasma gas is assumed to be in local thermodynamic equilibrium and optically thin. The flow is steady, laminar, axisymmetric with negligible viscous dissipation. The electromagnetic fields are assumed to be one dimensional. For the injected particles, the particle–particle interactions are neglected and no internal heat transfer in the particles is considered. The plasma gas is argon under atmospheric pressure. The transport properties of argon–copper mixtures are those of ref. [10]. For alumina powders, the transport properties of pure argon are used.

2.1. *The plasma equations*

The continuity, momentum, energy, and mass transfer equations in their general form can be expressed as follows:

$$\nabla \cdot \rho \mathbf{u} = S_p^c, \tag{1}$$

$$\rho \mathbf{u} \cdot \nabla \mathbf{u} = -\nabla p + \nabla \cdot \mu \nabla \mathbf{u} + \mathbf{J} \times \mathbf{B} + \mathbf{S}_p^M, \tag{2}$$

$$\rho \mathbf{u} \cdot \nabla h = \nabla \cdot \frac{k}{C_p} \nabla h + \sigma E^2 - Q_r + S_p^E, \tag{3}$$

$$\rho \mathbf{u} \cdot \nabla y = \nabla \cdot D \nabla y + S_p^c, \tag{4}$$

where S_p^c, $\mathbf{S}_p^M$, and S_p^E are the contributions of the particles to the transport of mass, momentum, and enthalpy respectively. A full listing of the corresponding transport equations in cylindrical coordinates, the electromagnetic field equations, and the boundary conditions used is given in the Appendix. Detailed descriptions of the numerical technique employed in solving equations (1)–(4) and also the corresponding electromagnetic field equations are given in [9]. The principal differences between the equations used in the present investigation and those given in [9] are the source terms which are modified to account for the plasma–particles interaction effects. The exact formulation of these terms are given in section 2.3.

NOMENCLATURE

$\mathbf{B}$	magnetic field intensity
Bi	Biot number, k/k_p
C	particle concentration in a cell
C_D	drag coefficient
c_p	specific heat at constant pressure
D	diffusion coefficient
d_p	particle diameter
E_θ	circumferential electric field intensity
F_r	body force in the radial direction
g	acceleration of gravity
h	enthalpy
h_c	heat transfer coefficient
H_m	latent heat of melting
H_v	latent heat of evaporation
H_z	axial magnetic field intensity
$\mathbf{J}$	current density
k	thermal conductivity
k_c	thermal conductivity of the quartz tube
$\dot{m}_p^0$	feed rate of particles [g min^{-1}]
$\dot{m}_v^0$	particle evaporation rate [g min^{-1}]
N_t^0	total number of particles injected per unit time
n_r	fraction of N_t^0 injected at each point
Nu	Nusselt number
P	pressure
Q	plasma gas flow rate
Q_r	radiation loss per unit volume
r	distance in the radial direction
R_0	inside radius of the tube
R_c	coil radius
Re	Reynolds number
S_p^c	particle source term in the continuity equation
S_p^E	particle source term in the energy equation
$\mathbf{S}_p^M$	particle source term in the momentum equation
S_p^{Mr}	radial component of $\mathbf{S}_p^M$
S_p^{Mz}	axial component of $\mathbf{S}_p^M$
t	time
T	temperature
T_a	ambient temperature
$\mathbf{u}$	gas velocity
u	axial velocity component
U_R	relative speed of particles with respect to plasma gas
v	radial velocity component
V	volume
w	tube wall thickness
x	liquid fraction of a particle
y	particles vapor concentration
z	distance in the axial direction.

Greek symbols

ε	emissivity of particle surface
ξ	magnetic permeability
ρ	density
σ	electrical conductivity
σ_p	standard deviation
σ_s	Stefan–Boltzmann constant
χ	phase angle $(\phi_H - \phi_E)$
ω	oscillator frequency
μ	viscosity
τ	residence time of particles in a cell.

Subscripts

p	particles
l	particles with initial diameter of d_l
k	particles injected at radius r_k
(i, j)	location of a typical cell.

Superscripts

(l, k)	particles having an initial diameter d_l, and injection point r_k.

2.2. *The particle trajectory equations*

Assuming that the only forces affecting an individual particle trajectory, are the drag and the gravity, the momentum equations for a single particle injected vertically downward into the plasma can be expressed as [4]:

$$\frac{du_p}{dt} = -\frac{3}{4} C_D (u_p - u) U_R \left(\frac{\rho}{\rho_p d_p}\right) + g \tag{5}$$

$$\frac{dv_p}{dt} = -\frac{3}{4} C_D (v_p - v) U_R \left(\frac{\rho}{\rho_p d_p}\right). \tag{6}$$

The particle temperature is determined by an energy balance:

$$Q = \pi d_p^2 h_c (T - T_p) - \pi d_p^2 \sigma_s \varepsilon (T_p^4 - T_a^4), \tag{7}$$

where Q is the net heat exchange between the particles and its surroundings,

$$Q = \begin{cases} \left(\frac{\pi}{6} \rho_p d_p^3 c_p\right) \frac{dT_p}{dt} & \text{for } T < T_m \text{ and } T_m < T < T_b \\ \left(\frac{\pi}{6} \rho_p d_p^3 H_m\right) \frac{dx}{dt} & \text{for } T = T_m \\ \left(-\frac{\pi}{2} \rho_p d_p^2 H_v\right) \frac{dd_p}{dt} & \text{for } T = T_b \end{cases} \tag{8}$$

and

$$U_R = \sqrt{(u_p - u)^2 + (v_p - v)^2}. \tag{9}$$

C_D is the drag coefficient, u_p and v_p are the axial and the radial particle velocities respectively, U_R is the relative

speed between the particle and the plasma gas, d_p is the particle diameter, h_c is the heat transfer coefficient, ε is the particle emissivity, x is the liquid mass fraction of the particle, and T_p, T_m, T_b are the particle temperature, melting point temperature, and the boiling temperature respectively. The drag coefficient C_D, and the heat transfer coefficient h_c, are estimated using the following relations [4]:

$$C_D = \begin{cases} \dfrac{24}{Re} & Re \leqslant 0.2 \\ \dfrac{24}{Re}\left(1+\dfrac{3}{16}Re\right) & 0.2 < Re \leqslant 2.0 \\ \dfrac{24}{Re}\left(1+0.11\,Re^{0.81}\right) & 2.0 < Re \leqslant 21.0 \\ \dfrac{24}{Re}\left(1+0.189\,Re^{0.62}\right) & 21.0 < Re \leqslant 200 \end{cases} \tag{10}$$

and

$$Nu = \frac{h_c d_p}{k} = 2.0 + 0.515\,Re^{0.5} \tag{11}$$

where Re is the Reynolds number based on the particle diameter and the relative speed between the particle and the gas, U_R.

2.3. *The source terms*

In this part the formulation of the source terms S_p^c, S_p^M, and S_p^E [equations (1)–(4)] is given.

Let N_t^0 be the total number of particles injected per unit time, n_d is the particle size distribution, and n_r represents the fraction of N_t^0 injected at each point over the central tube radius (Fig. 1). The total number of particles per unit time travelling along the trajectory (l, k) corresponding to a particle diameter d_p injected at the point r_k is:

$$N^{0(l,k)} = n_{dl} n_{rk} N_t^0. \tag{12}$$

The distribution of n_d is assumed to be Gaussian. For n_r, we assume that the particle concentration in the central tube is uniform. For the sake of computations the distributions n_d and n_r are discretized into seven particle diameters and five injection points respectively, giving rise to 35 different possible particles trajectories. The injection velocity of the particles is assumed to be equal to the velocity of the central carrier gas at the point of injection.

The particle concentration in a given cell crossed by the trajectory (l, k) is:

$$C_{ij}^{(l,k)} = \frac{N^{0(l,k)} \tau_{ij}^{(l,k)}}{V_{ij}}. \tag{13}$$

Where $\tau_{ij}^{(l,k)}$ is the residence time of the (l, k) particles in the (ij) cell of volume V_{ij}. The mass source term for the (ij) cell, due to all the trajectories with initial diameter d_l

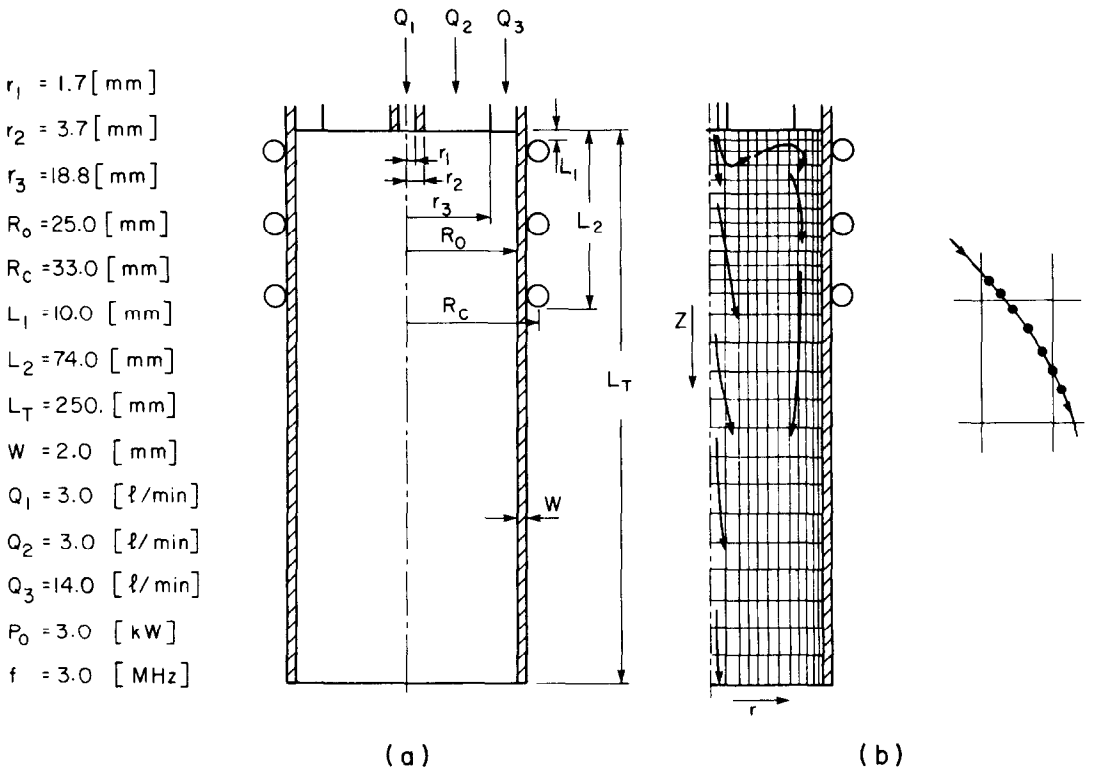

FIG. 1. (a) Schematics of the torch and its operating conditions. (b) Computational domain and a typical cell.

and initial injection point r_k is given as:

$$S^{c}_{p,ij} = \sum_{l,k} C^{(l,k)}_{ij} \frac{\Delta m^{(l,k)}_{p}}{\tau^{(l,k)}_{ij}} \tag{14}$$

$\Delta m^{(l,k)}_{p}$ is the amount of mass evaporated by a particle with (l,k) trajectory in cell (ij). The corresponding source term in the energy equation includes the heat given to the particles $Q^{(l,k)}_{p,ij}$, as well as the superheat needed to bring the particle vapors into thermal equilibrium with the plasma gas $Q^{(l,k)}_{v,ij}$:

$$S^{E}_{p,ij} = \sum_{l,k} C^{(l,k)}_{ij} [Q^{(l,k)}_{p,ij} + Q^{(l,k)}_{v,ij}] \tag{15}$$

where

$$Q^{(l,k)}_{p,ij} = \frac{1}{\tau^{(l,k)}_{ij}} \int_{0}^{\tau^{(l,k)}_{ij}} \pi d_p^2 h_c [T_{ij} - T^{(l,k)}_{p,ij}] \, dt \tag{16}$$

and

$$Q^{(l,k)}_{v,ij} = \frac{1}{\tau^{(l,k)}_{ij}} \int_{0}^{\tau^{(l,k)}_{ij}} \frac{\pi}{2} d_p^2 \rho_p \left(\frac{d d_p}{dt}\right) c_{p_v} \times [T_{ij} - T^{(l,k)}_{p,ij}] \, dt \tag{17}$$

S^{M}_{p} has two components, i.e. radial S^{Mr}_{p} and axial S^{Mz}_{p}:

$$S^{Mr}_{p,ij} = \sum_{(l,k)} C^{(l,k)}_{ij} \frac{\Delta(m_p v_p)}{\tau^{(l,k)}_{ij}} \tag{18}$$

and

$$S^{Mz}_{p,ij} = \sum_{(l,k)} C^{(l,k)}_{ij} \frac{\Delta(m_p u_p)}{\tau^{(l,k)}_{ij}}. \tag{19}$$

The system of equations (1)–(8) with the auxiliary relations (12)–(19) are solved iteratively for the torch geometry and operating conditions given in Fig. 2. A schematic diagram of the grid used and a typical cell is also included in Fig. 1, while a block diagram of the iterative procedure is given in Fig. 2.

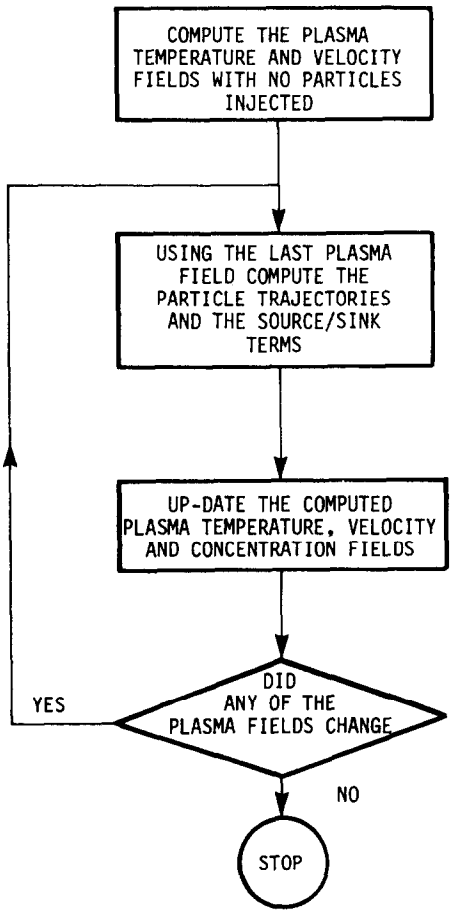

FIG. 2. Flow chart of the computational method.

3. RESULTS AND DISCUSSION

Computations are carried out for an inductively-coupled plasma torch operated with argon at atmospheric pressure and at a power level of 3 kW. The oscillator's frequency is 3 MHz and the total argon flow rate is 20 dm^3 min^{-1}.

Two cases are investigated. In the first case copper powder with a mean particle diameter of 70 μm and a standard deviation of 30 μm is injected through the central tube into the coil region of the discharge. The choice of copper powder enable us to study an important effect of particle–plasma interactions. Mostaghimi and Pfender [7] have shown that the presence of even minute amounts of copper will change the electrical properties of argon dramatically. Because of the low boiling point of copper, copper evaporates easily and the vapor diffuses into the plasma gas and changes its properties. For the second case, alumina powder with a mean particle diameter of 70 μm and a standard deviation of 30 μm is injected into the torch. Alumina has completely different thermophysical properties to copper. A summary of the thermophysical properties of copper and alumina is given in Table 1. Table 2 shows the particle size distributions, their feed-rate, and their overall evaporation and energy absorption. For the argon–copper case, the transport properties used are those of ref. [7] whereas for argon–alumina case, the transport properties of pure argon are used.

3.1. *Case 1*

In this case copper is injected downward through the central tube into the torch. The parameters investigated are:

(a) Effect of particle loading.
(b) Effect of particle size.
(c) Effect of the central carrier gas flow rate.

Effect of particle loading. In this case copper is injected at a rate of 1.0–20.0 g min^{-1}. Figures 3 and 4 show the isotherms, stream lines, and the concentration of copper vapor in the torch for 5 and 15 g min^{-1} of copper feed-rate respectively. A comparison of the two figures shows the cooling effect that the increase in the copper feed-rate causes. Because the trajectories of the

Table 1. Thermophysical properties of copper and alumina powders

	T_m (K)	T_b (K)	H_m (kJ kg^{-1})	H_v (kJ kg^{-1} K^{-1})	c_p (kJ kg^{-1} K^{-1})	c_{p_v} (kJ kg^{-1} K^{-1})	ρ_p (kg m^{-3})
copper	1356	2840	200	5000	0.425	0.480	8900
alumina	2323	3800	1000	25000	1.500	0.960	3900

Table 2. Particle size distribution, feed-rate, and energy absorbed by powders

Material	$\overline{d_p}$ (μm)	σ_p (μm)	$\dot{m}_p^0$ (g min^{-1})	$\dot{m}_v^0$ (g min^{-1})	Q_p (W)	Q_v (W)	% of total energy absorbed
copper	70	30	1.0	0.50	71.0	21.0	3.1
	70	30	5.0	1.40	255.0	42.0	9.9
	70	30	10.0	1.40	386.0	35.0	14.0
	70	30	15.0	1.16	460.0	28.0	16.3
	70	30	20.0	0.94	511.0	23.0	17.8
	70	3	10.0	1.60	415.0	36.0	15.0
	90	3	10.0	0.70	319.0	15.0	11.1
alumina	70	30	5.0	0.10	412.0	4.0	13.9
	70	30	10.0	—	530.0	—	17.7
copper	90	30	0.5	0.36	56.0	16.0	2.4

particles are very close to the axis, the plasma gas is significantly cooled down in this region (Fig. 5). However, the outer region of the plasma, where most of the power is dissipated, remains largely unaffected by the increase in the copper feed-rate (Fig. 6). This result clearly demonstrates that although the loading ratio of copper to plasma gas might be small, the local cooling effects could be very significant. For example, consider the case of $\dot{m}_p^0 = 5$ g min^{-1}. The mass loading ratio is about 0.19 g copper/g argon and the temperature on the axis has dropped by about 2000 K. In other words, the

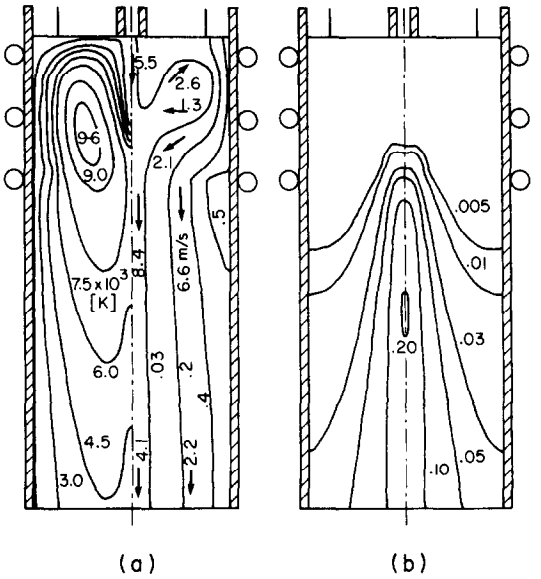

FIG. 3. (a) Isotherms and stream lines for 5.0 g min^{-1} copper feed-rate. (b) Iso-concentration contours of copper vapor for this case.

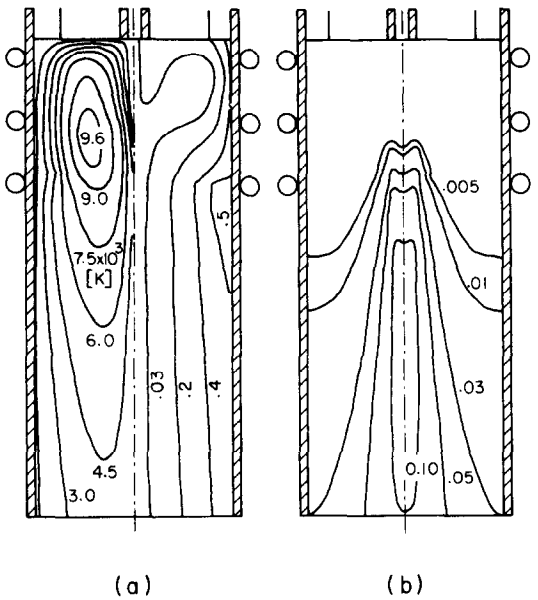

FIG. 4. Same as in Fig. 3 for a copper feed-rate of 15.0 g min^{-1}.

plasma–particle interactions could locally be very important under the loading conditions which are generally assumed to be safe to neglect the changes in plasma temperature due to the presence of powders.

Momentum transfer between the gas and the particles is found to be negligible and the flow field is affected only through the local plasma temperature changes, i.e. the temperature changes will change the local transport properties. As the particles pass through the plasma, a portion of them evaporates (Table 2), and the vapor diffuses into the plasma medium (Figs. 3–4). The heat absorbed by the solid particles Q_p, and the

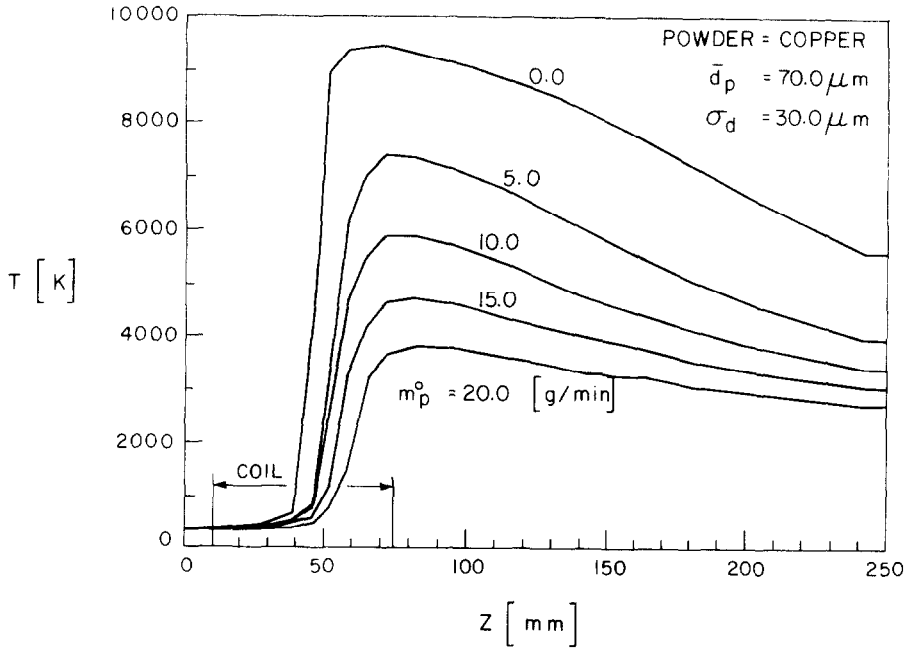

FIG. 5. Effect of particle feed-rate on the temperature profile along the axis of the torch.

superheat absorbed by the copper vapor to heat up to the plasma temperature Q_v, are given in Table 2. Q_v is generally much smaller than Q_p, the ratio Q_v/Q_p changes from 29.6% at 1 g min^{-1} feed-rate to 4.5% at 20 g min^{-1} feed-rate, and the total energy absorbed by the powder is between 3.1 and 17.8% of the plasma power input.

The presence of copper vapor can change the electrical conductivity of argon significantly. Mostaghimi and Pfender show that for an argon plasma contaminated with 1.0% copper vapor, the electrical conductivity at $T = 5000$ K increases by a factor of 28. Under the conditions of this section, the copper vapor is formed after the coil region and therefore the electrical conductivity in this zone is not changed.

Effect of particle size. The Gaussian distribution of the particle diameters is characterized by their average diameter and standard deviation. These parameters are

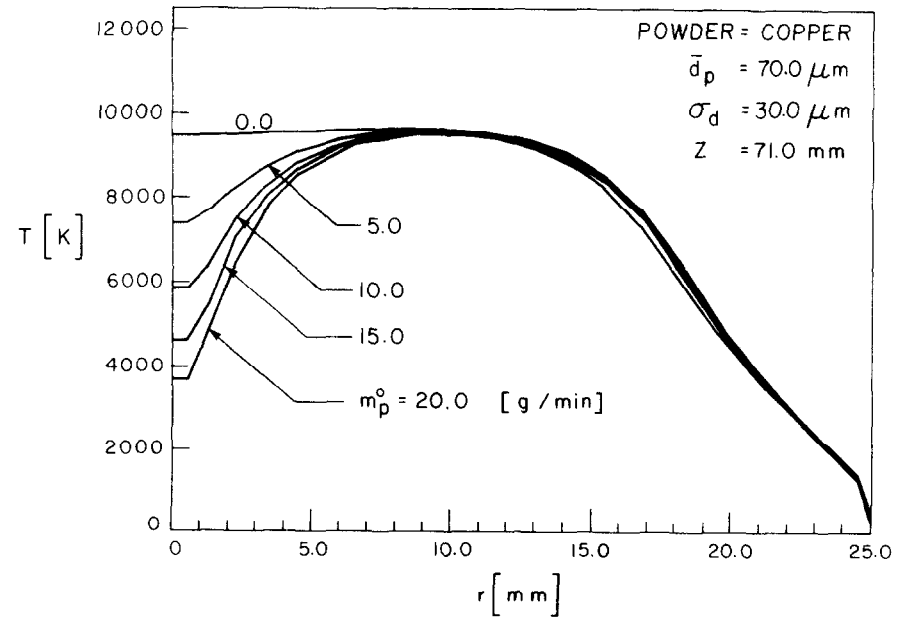

FIG. 6. Effect of particle feed-rate on the radial temperature profile at $z = 71.0$ mm.

varied (Table 2) to simulate the effect of different particle size distribution. While it is not quite evident from the data given in Table 2, the results of the computations generally indicate that a very wide particle size distribution results in a poor treatment of the powder, i.e. large particles are not treated and the very small ones are completely evaporated. The presence of particles of diameters less than 10 μm, has also been noted to substantially increase the cooling effect of the particles on the plasma gas due to the rapid evaporation of the small particles.

Effect of the central carrier gas. The central carrier gas flow-rate is an important factor in determining the trajectories of the particles. When the central flow-rate is high enough, e.g. 3 dm^3 min^{-1} for the present torch, particles will easily go through the discharge. The recirculation which is characteristic of an inductively coupled plasma is then restricted to a small doughnut-shaped region of the central axis. However, for lower central flow-rates, the recirculation zone is expanded and it repells the particles injected in the center. This causes a drastic change in the pattern of the trajectories. For example, it is noted that for 1.0 dm^3 min^{-1} central flow-rate, the particles bounce off the plasma and are entrained outward by the recirculation and penetrate the plasma region with the sheath gas. This has been schematically demonstrated in Fig. 1. Although very few copper particles enter the discharge zone, a significant amount of copper vapor will be present in this region due to the electromagnetic pumping effect, i.e. $\mathbf{J} \times \mathbf{B}$ force.

Figures 7(a) and (b) show the flow and the temperature fields for 1.0 dm^3 min^{-1} central flow-rate and no copper injected [Fig. 7(a)], and 0.5 g min^{-1} copper feed-rate [Fig. 7(b)]. It is found that a uniform concentration of 1.7% copper vapor exists in the discharge region. Because of the low particle feed-rate, the absorption of energy by the particles from the plasma is small (3.1%). However, the presence of copper vapor in the discharge zone causes the high temperature zone, i.e. $T > 9600$ K to disappear. This is mainly due to the changes in the electrical conductivity of the plasma gas as a result of the copper vapor cloud. Figure 8 obtained from ref. [7] shows the dependence of argon electrical conductivity on the amount of the copper vapor in the plasma. The increase in the electrical conductivity changes the energy distribution in the discharge zone and results in reducing the maximum temperature of the discharge.

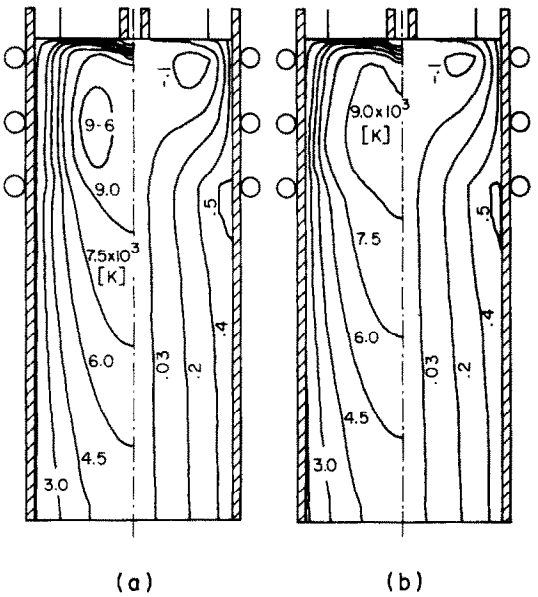

FIG. 7. Effect of copper vapor on the temperature and flow fields of the torch (Q = 1.0 dm^3 min^{-1}). (a) No particles injected. (b) 0.5 g min^{-1} of copper injected.

3.2. *Case 2*

In order to investigate the effect of the thermophysical properties of the powders on the plasma–particle interactions, results for an alumina powder are obtained. The properties of alumina, as demonstrated in Table 1, is quite different than the copper particles. Its melting and boiling temperatures, the corresponding latent heat and its specific heat are much larger than those of copper whereas its density is smaller.

The low thermal conductivity of alumina could lead to high internal temperature gradients. Bourdin *et al.* [1] have proposed that if the Biot number is less than 0.02, the temperature gradients inside the particles can be neglected. For alumina particles in an argon plasma, the Biot number is found to be 0.04, and the temperature difference between the particle surface and its center will be less than 10% of the temperature difference between the particle surface and the plasma temperature [1].

Table 2 shows the results for 5.0 g min^{-1} and 10.0 g min^{-1} feed-rate of alumina powder into the torch. For the same powder feed-rate the energy absorbed by alumina is significantly higher than the energy absorbed by copper. For example the energy absorbed by alumina at a rate of 5 g min^{-1} is almost equal to the absorbed energy by the copper particles fed at a rate of 10.0 g min^{-1}. The reason for this is that the high melting and boiling points of alumina makes the particles more difficult to evaporate and therefore they have longer time to exchange heat with the plasma. The amount of alumina evaporated is found to be very small (Table 2). Because of the small amount of evaporation of alumina and also the unknown dependence of the argon properties on these concentrations, we have used the properties of pure argon for this case.

4. CONCLUSIONS

The Particle-Source-In-Cell (PSI-Cell) method is applied to the problem of injecting powders into an inductively coupled plasma torch. It is found that the effect of plasma–particle interaction on the temperature field could be very significant. The results indicate

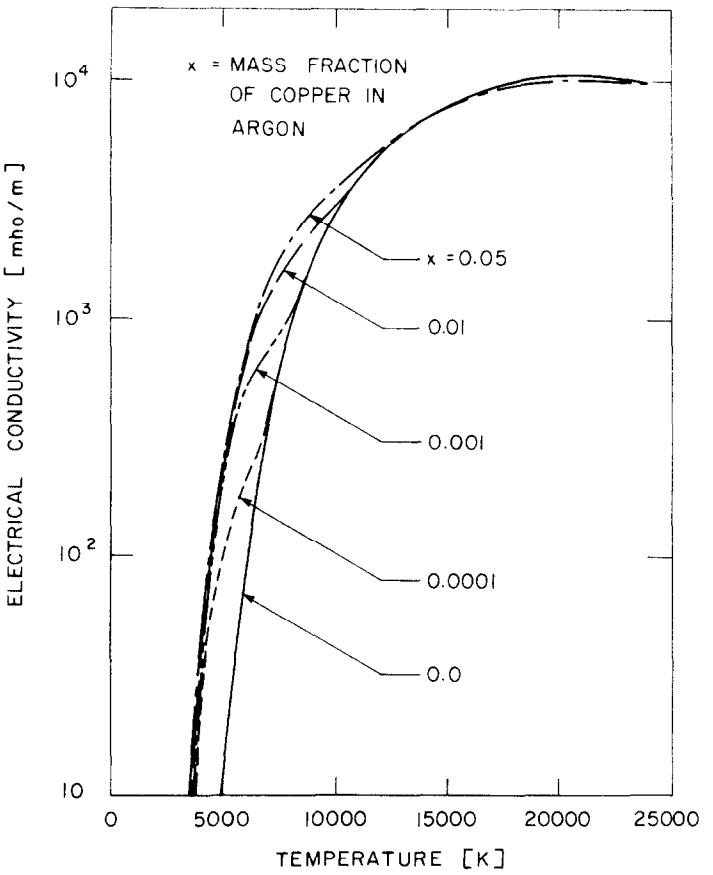

FIG. 8. Effect of copper vapor on the electrical conductivity of argon at 1.0 atm.

that for the operating conditions and powder feed-rates used in this paper, up to 18% of the total energy dissipated in the torch can be absorbed by the particles. This will cause significant local cooling of the plasma gas. It also underlines that neglecting the plasma–particle interactions where it seems to be appropriate, could be unrealistic. It is found that powders with large number of small particles will absorb more heat than powders which are composed of larger particles.

The thermophysical properties of the particles are also an important factor in this problem. It is found that for the same feed-rate, alumina absorbs much more energy than copper.

Another conclusion is that the evaporated powder might play an important role in altering the electrical properties of the gas and thus change the energy dissipation pattern and tend to moderately cool the plasma core.

Finally, it is demonstrated that the central gas flow-rate is a determining factor in the trajectory that the particles follows. Low central flow-rates cause the particles to travel around the recirculating zone whereas high central flow-rates keep the particles very close to the central axis.

Acknowledgement—This work was partially supported by a subcontract from the University of Massachusetts, Amherst, recipient of Department of Energy (Office of Basic Energy Sciences) contract DE-AC02-77ER4471, Ramon M. Barnes, principal investigator. The support by the Ministry of Education of the Province of Québec and the Natural Sciences and Engineering Research Council of Canada is gratefully acknowledged.

REFERENCES

1. E. Bourdin, P. Fauchais and M. I. Boulos, Transient heat conduction under plasma conditions, *Int. J. Heat Mass Transfer* **26**, 567–582 (1983).
2. M. Vardelle, A. Vardelle, P. Fauchais and M. I. Boulos, Plasma–particle momentum and heat transfer: modelling and measurements, *A.I.Ch.E. Jl* **29**, 236–242 (1983).
3. J. K. Fiszdon, Melting of powder in a plasma flame, *Int. J. Heat Mass Transfer* **22**, 749–761 (1979).
4. M. I. Boulos, Heating of powders in the fire ball of an induction plasma, *IEEE Trans. Plasma Sci.* **PS-6**, 93–106 (1978).
5. C. Borgianni, M. Capitelli, F. Cramarossa, L. Triolo and E. Molinari, The behaviour of metal oxides injected into an argon induction plasma, *Combust. Flame* **13**, 181–194 (1969).
6. T. Yoshida and K. Akashi, Particle heating in a radio-frequency plasma torch, *J. appl. Phys.* **48**, 2252–2260 (1977).
7. J. Mostaghimi and E. Pfender, Effects of metallic vapor on the properties of an argon arc plasma, *Plasma Chem. Plasma Process.* **4**, 199–217 (1984).
8. C. T. Crowe, M. P. Sharma and D. E. Stock, The Particle-Source-In-Cell (PSI-Cell) model for gas-droplet flows, *J. Fluids Engng* **99**, 325–332 (1977).
9. J. Mostaghimi, P. Proulx and M. I. Boulos, An analysis of the computer modeling of the flow and temperature fields in an inductively coupled plasma, *J. numer. Heat Transfer* **8**, 187–201 (1985).

APPENDIX

Definition of all the symbols used is given in the nomenclature.

1. *The plasma equations*

1.1. *Continuity.*

$$\frac{1}{r}\frac{\partial}{\partial r}(r\rho v)+\frac{\partial}{\partial z}(\rho u)=S_p^c. \tag{A1}$$

1.2. *Momentum transfer equations.*

$$\rho\left\{v\frac{\partial u}{\partial r}+u\frac{\partial u}{\partial z}\right\}=-\frac{\partial p}{\partial z}+2\frac{\partial}{\partial z}\left(\mu\frac{\partial u}{\partial z}\right)+\frac{1}{r}\frac{\partial}{\partial r}\left\{\mu r\left(\frac{\partial v}{\partial r}+\frac{\partial u}{\partial r}\right)\right\}+\rho g+S_p^{Mz} \tag{A2}$$

$$\rho\left\{v\frac{\partial v}{\partial r}+u\frac{\partial v}{\partial z}\right\}=-\frac{\partial p}{\partial r}+\frac{2}{r}\frac{\partial}{\partial r}\left(\mu r\frac{\partial v}{\partial r}\right)+\frac{\partial}{\partial z}\left\{\mu\left[\frac{\partial v}{\partial z}+\frac{\partial u}{\partial r}\right]\right\}-\frac{2\mu v}{r^2}+Fr+S_p^{Mr}. \tag{A3}$$

1.3. *Energy transfer equation.*

$$\rho\left(v\frac{\partial h}{\partial r}+u\frac{\partial h}{\partial z}\right)=\frac{1}{r}\frac{\partial}{\partial r}\left(r\frac{k}{c_p}\frac{\partial h}{\partial r}\right)+\frac{\partial}{\partial z}\left(\frac{k}{c_p}\frac{\partial h}{\partial z}\right)+P-Q_r+S_p^E. \tag{A4}$$

1.4. *Mass transfer equation.*

$$\rho\left(v\frac{\partial y}{\partial r}+u\frac{\partial y}{\partial z}\right)=\frac{1}{r}\frac{\partial}{\partial r}rD\frac{\partial y}{\partial r}+\frac{\partial}{\partial z}\left(D\frac{\partial y}{\partial z}\right)+S_p^c. \tag{A5}$$

2. *Electromagnetic field equations*

$$\frac{1}{r}\frac{d}{dr}(rE_\theta)=-\zeta\omega H_z\sin\chi \tag{A6}$$

$$\frac{dH_z}{dr}=-\sigma E_\theta\cos\chi \tag{A7}$$

$$\frac{d\chi}{dr}=\frac{\sigma E_\theta}{H_z}\sin\chi-\frac{\zeta\omega H_z}{E_\theta}\cos\chi \tag{A8}$$

with $P=\sigma E_\theta^2$ volumetric rate of heat generation due to Joule heating and $F_r=-\zeta\sigma E_\theta H_z\cos\chi$ the radial body force acting on the plasma gas in the discharge region.

3. *Boundary conditions*

Inlet conditions (z = 0).

$v=0$

$$u=\begin{cases}Q_1/\pi r_1^2 & r<r_1\\ 0.0 & r_1\leqslant r\leqslant r_2\\ Q_2/\pi(r_3^2-r_2^2) & r_2<r\leqslant r_3\\ Q_3/(R_0^2-r_3^2) & r_3<r\leqslant R_0\end{cases} \tag{A9}$$

$T=350$ K

$y=0.$

Centerline (r = 0).

$$v=0,\quad \frac{\partial u}{\partial r}=0,\quad \frac{\partial h}{\partial r}=0,\quad \frac{\partial y}{\partial r}=0. \tag{A10}$$

Wall ($r=R_0$).

$$u=v=0,\quad \frac{k}{c_p}\frac{\partial h}{\partial r}=\frac{k_c}{w}(T-T_{wo}),\quad \frac{\partial y}{\partial r}=0 \tag{A11}$$

where T_{wo}, the external surface temperature of the tube, $T_{wo}=350$ K.

Exit ($z=L_T$). The boundary condition at this section is not known. However, if the exit Peclet number, i.e. *Re Pr*, is sufficiently large, one can safely assume the following:

$$\frac{\partial h}{\partial z}=0,\quad \frac{\partial v}{\partial z}=0,\quad \frac{\partial(\rho u)}{\partial z}=0,\quad \frac{\partial y}{\partial z}=0. \tag{A12}$$

The boundary conditions for the electromagnetic field are set at $r=0$ and $L_1\leqslant Z\leqslant L_2$ is:

$$\chi=\frac{\pi}{2},\quad E_\theta=0,\quad H_z=H_{c\infty}\left\{\frac{L_2-z}{[R_c^2+(L_2-z)^2]^{1/2}}-\frac{L_1-z}{[R_c^2+(L_1-z)^2]^{1/2}}\right\} \tag{A13}$$

where $H_{c\infty}$ is the magnetic field intensity for an infinite solenoid.

$$H_{c\infty}=\frac{NI}{L_2-L_1}. \tag{A14}$$

It is to be noted that $H_{c\infty}$ is not specified, rather the total power input to the plasma, P_0, is known. This is set as an integral type boundary condition.

$$P_t=\int_{z=L_1}^{L_2}\int_{r=0}^{R_0}2\pi r\,P\,dr\,dz \tag{A15}$$

and if $P_t\neq P_0$, a correction factor to the electric field and magnetic field is found:

$$\alpha_c=\sqrt{\frac{P_0}{P_t}} \tag{A16}$$

multiplying the electromagnetic fields by α_c insures that the conditions $P_t=P_0$ is satisfied.

EFFETS D'INTERACTION PLASMA–PARTICULE DANS LA MODELISATION DU PLASMA AVEC INDUCTION SOUS DES CONDITIONS DE CHARGE DENSE

Résumé—On modélise l'injection de poudres dans un plasma couplé par induction. L'attention est portée sur l'interaction plasma–particule et son effet sur les champs de plasma. On démontre que, pour la plupart des applications, de telles interactions peuvent être considérées dans un modèle quelconque. Pour les calculs, on considère des poudres de cuivre et d'aluminium. Le plasma est de l'argon à la pression atmosphérique.

DIE WECHSELWIRKUNG VON PLASMA–PARTIKELN BEI DER MODELLIERUNG VON INDUKTIONS-PLASMA VON HOHER DICHTE

Zusammenfassung—Der Einsprühvorgang von Staub in ein induktiv eingekoppeltes Plasma wird modelliert. Die Wechselwirkung der Plasma–Partikel und deren Einfluß auf die Plasmafelder wird berücksichtigt. Es wird gezeigt, daß für die meisten Anwendungen solche Wechselwirkungen in jedem Modell berücksichtigt werden müssen. Die Berechnungen wurden für Kupfer- und Aluminiumstaub durchgeführt. Das Plasmagas ist Argon bei Umgebungsdruck.

ЭФФЕКТЫ ВЗАИМОДЕЙСТВИЯ ИНДУКЦИОННОЙ ПЛАЗМЫ С ЧАСТИЦАМИ ПРИ МОДЕЛИРОВАНИИ В УСЛОВИЯХ СИЛЬНОГО НАГРУЖЕНИЯ

Аннотация—Моделируется введение порошков в индукционную плазму. Внимание уделяется взаимодействию плазмы с частицами и его влиянию на плазму. Показано, что для большинства применений такие взаимодействия должны рассматриваться в любой модели. Расчеты проведены для медного и алюминиевого порошков. В качестве плазменного газа используется аргон при атмосферном давлении.